

## **Electronic Supplementary Information**

### **Two-dimensional IV-VA<sub>3</sub> monolayers with enhanced charge mobility for high-performance solar cells**

Meiqiu Xie,<sup>a</sup> Yang Li,<sup>a</sup> Xuhai Liu,<sup>b</sup> Jianping Yang,<sup>a</sup> Hui Li<sup>a,\*</sup> and Xing'ao Li<sup>a,c,\*</sup>

<sup>a</sup>*New Energy Technology Engineering Laboratory of Jiangsu Province & School of Science,  
Nanjing University of Posts and Telecommunications (NJUPT), Nanjing 210023, China*

<sup>b</sup>*College of Microtechnology & Nanotechnology, Qingdao University, Qingdao 266071, China*

<sup>c</sup>*School of Science, Zhejiang University of Science and Technology, Hangzhou 310023, China*

**\*E-mail addresses:** lihui1986@njupt.edu.cn (H. Li), lixa@njupt.edu.cn (X. Li).

## List

### THEORETICAL METHODS

S1 Cohesive energy

S2 Optical absorption coefficient and details of GW+BSE calculation

S3 Carrier mobility

S4 Power conversion efficiency

Fig. S1 The 2D and 3D ELFs of monolayer SiX<sub>3</sub> (X=P, As, Sb) are presented.

Fig. S2 The 2D and 3D ELFs of monolayer GeX<sub>3</sub> (X=P, As, Sb) are presented.

Fig. S3 Side and top views of nine stacked (AAA, AAB, AAC, ABA, ABB, ABC, ACA and ACB) bulk AX<sub>3</sub> (X=P, As, Sb). The pink lines in the bottom panels of every stacked structure stand for the rhombus primitive cell.

Fig. S4 The cleavage energies of monolayer AX<sub>3</sub>, coupled with blue phosphorene, black phosphorene, grey antimonene, monolayer MoS<sub>2</sub> and graphene for comparison.

Fig. S5 Electronic band structures of monolayer AX<sub>3</sub> (A=Si, Ge; X=P, As, Sb). Red and blue lines represent the CB and VB near to the Fermi Level based on PBE functional, respectively.

Fig. S6 The projected density of states of monolayer SiX<sub>3</sub> (a) and GeX<sub>3</sub> (b) (X=P, As).

Fig. S7 Temperature and total energy during an ab initio molecular dynamics (AIMD) simulation of monolayer SiX<sub>3</sub> (a) and GeX<sub>3</sub> (b) (X=P, As) at 300 K. Inset: atomic structure after 5.0 ps.

Fig. S8 (a) Atomic structure model of monolayer AX<sub>3</sub> (X=P, As). The dashed lines represent the rhombus primitive cell and the rectangular supercell. Electronic band structures of monolayer SiP<sub>3</sub> (b), and SiAs<sub>3</sub> (c), GeP<sub>3</sub> (d) and GeAs<sub>3</sub> (e) in the orthogonal supercell.

Fig. S9 2D elastic constant evaluation for the SiP<sub>3</sub> (a), SiAs<sub>3</sub> (b), GeP<sub>3</sub> (c) and GeAs<sub>3</sub> (d) monolayers. Total energy with respect to the lattice dilation  $\Delta l/l_0$ . The polynomial fit of the data gives the 2D elastic constant.

Fig. S10 SiP<sub>3</sub>/ZnO (a), SiAs<sub>3</sub>/MoTe<sub>2</sub> (b) and GeAs<sub>3</sub>/WS<sub>2</sub> (c) type-II semiconductor heterojunctions.

(d) Projected electronic structure of SiAs<sub>3</sub>/MoTe<sub>2</sub> heterojunction calculated using HSE06 functional.

Fig. S11 The devices structures of SiP<sub>3</sub>- (a), SiAs<sub>3</sub>- (b) and GeAs<sub>3</sub>-based (c) single-junction SCs.

Fig. S12 (a) Energy diagram of the band alignment (HSE06 functional) for SiP<sub>3</sub>-, SiAs<sub>3</sub>- and GeAs<sub>3</sub>-based single-junction SCs with 22.15%, 18.52% and 18.08% efficiency, respectively. (b)

Thermalization loss and below- $E_g$  loss in the SiP<sub>3</sub>-, SiAs<sub>3</sub>- and GeAs<sub>3</sub>-based single-junction SCs.

Table S1 Structural parameters and electronic properties for relaxed AX<sub>3</sub> monolayers.

Table S2. Calculated cohesive energy differences ( $\Delta E_{coh}$ ) are given in units of eV.  $\Delta E_{coh}$  is based on the ABC stacking AX<sub>3</sub> monolayer calculated with PBE functional.

Table S3 Effective mass  $m_i^*/m_0$ , DP constant  $E_{li}$  in eV, elastic constant  $C_{2D}$  in Jm<sup>-2</sup>, and carrier mobility  $\mu$  in cm<sup>2</sup>V<sup>-1</sup>s<sup>-1</sup>, at 300 K for electrons and holes in monolayer AX<sub>3</sub> (A=Si, Ge; X=P, As). (x=zigzag, y=armchair)

Table S4 Confirmed existing SCs and the PCE measured under the global AM1.5 spectrum (1000 Wm<sup>-2</sup>).

## S1. Cohesive energy

$$E_{Coh} = \frac{nE_A + 3nE_X - E_{total}}{4n}$$

(S1)

$E_{total}$ ,  $E_A$  and  $E_X$  represent the total energies of  $AX_3$  ( $A=Si, Ge$ ;  $X=P, As, Sb$ ) monolayers, single atoms A and X, respectively.

## S2. Optical absorption coefficient and details of GW+BSE calculation

The calculated optical absorption properties rely on the complex dielectric function.

The imaginary part ( $\varepsilon_2(\omega)$ ) of the dielectric matrix can be obtained as<sup>1</sup>

$$\varepsilon_2(\omega) = \frac{4\pi^2 e^2}{\Omega} \lim_{q \rightarrow 0} \frac{1}{q^2} \sum_{c,v,k} 2w_k \delta(\vec{\Omega}_{ck} - \vec{\Omega}_{vk} - \omega) \times \left\langle u_{ck+e_\alpha} | u_{vk} \right\rangle \left\langle u_{ck+e_\beta} | u_{vk} \right\rangle^* \quad (S2)$$

where  $\Omega$  is the primitive cell volume, and  $w_k$  is the k-point weight. The indices  $c$  and  $v$  denote the conduction and valence band states, respectively.  $\epsilon$  is the band energy, and  $u$  is the cell periodic part of the orbitals at the k-point  $k$ . The vectors  $e_\alpha$  and  $e_\beta$  stand for unit vectors for the three Cartesian directions. The real part of dielectric function  $\varepsilon_1(\omega)$  is obtained from the imaginary part  $\varepsilon_2(\omega)$  using the Kramers-Kronig transformation<sup>1</sup>

$$\varepsilon_1(\omega) = 1 + \frac{4}{\pi} P \int_0^\infty \frac{\varepsilon_2(\omega') \omega'}{\omega'^2 - \omega^2 + i\eta} d\omega' \quad (S3)$$

where  $P$  is the principle value. Then, the optical absorption coefficient  $\alpha(\omega)$  is calculated based on both imaginary and real parts as following<sup>2</sup>

$$\alpha(\omega) = \sqrt{2\omega} \left[ \sqrt{\varepsilon_1^2(\omega) + \varepsilon_2^2(\omega)} - \varepsilon_1(\omega) \right]^{1/2} \quad (S4)$$

The optical absorption and excitonic effect concerned properties were carried out by the GW plus Bethe-Salpeter equation calculation (GW+BSE)<sup>3-5</sup>. Due to the interaction in periodic boundary conditions of  $AX_3$  monolayers, the Wigner-Seitz cell truncation was adopted.<sup>6</sup> The total number of bands set to 600 while calculating the dielectric function and quasi-particle (QP) energy, which guaranteed the QP bandgaps converged to 0.05 eV. The exciton wave functions and coupled electron-hole excitation energies were contained by solving BSE method. The 10 occupied and 16 unoccupied

bands were performed in constructing the electron-hole interaction kernel.

### S3. Carrier mobility

In inorganic semiconductors, the coherent wavelength of thermally activated electrons or holes at room temperature is much longer than the lattice constant and is close to the acoustic phonon wavelength. The electron-acoustic phonon coupling, leading to scattering in the low energy region, can be obtained based on deformation potential (DP) theory, which is first proposed by Bardeen and Shockley.<sup>7</sup> By means of the effective mass approximation, the DP theory has been widely used to investigate carrier mobility  $\mu$  in 2D materials:

$$\mu_{2D} = \frac{e\hbar^3 C_{2D}}{K_B T m_e^* m_d (E_1^i)^2}$$

(S5)

where,  $m_e^*$  is the effective mass in the transport direction;  $m_d$  is the average effective mass determined by  $m_d = (m_x^* m_y^*)^{1/2}$ .  $T$  is the temperature.  $C_{2D}$  is the DP constant which characterizes the shift of the band edges (the bottom of conduction band for electrons and the top of valence for holes) induced by the strain and is defined as  $E_{1i} = \Delta E_i / (\Delta l / l_0)$ .  $C_{2D}$  is the elastic modulus of  $x$  (zigzag) and  $y$  (armchair) uniformly deformed crystal for emulating the lattice distortion activated by the strain. For the 2D models the in-plane stiffness can be determined as  $C_{2D} = [\partial^2 E / \partial \delta^2] / S_0$ , here  $E$  is the total energy of the supercell,  $\delta$  is the applied uniaxial strain, and  $S_0$  is the area of the equilibrium supercell.

### S4. Power conversion efficiency

The power conversion efficiency PCE ( $\eta$ ) of such a  $AX_3$  and B (ZnO, MoTe<sub>2</sub> and WS<sub>2</sub>) described as<sup>8</sup>

$$\eta = \frac{J_{sc} V_{oc} \beta_{FF}}{P_{solar}} = \frac{0.65(E_g^d - \Delta E_c - 0.3) \int_{E_g^d}^{\infty} \frac{P(\hbar\omega)}{\hbar\omega} d(\hbar\omega)}{\int_0^{\infty} P(\hbar\omega) d(\hbar\omega)}$$

(S6)

where 0.65 is the fill factor  $\beta_{FF}$ ,  $P(\hbar w)$  is AM1.5 solar energy flux (stated in  $\text{Wm}^{-2}\text{eV}^{-1}$ )<sup>9</sup> at the photon energy ( $\hbar w$ ), and  $E_g^d$  is the band gap of the donor ( $\text{AX}_3$ ).  $\Delta E_c$  is the conduction band offset between donor ( $\text{SiP}_3$ ,  $\text{SiAs}_3$ ,  $\text{GeAs}_3$ ) and acceptor ( $\text{ZnO}$ ,  $\text{MoTe}_2$ ,  $\text{WS}_2$ ). The  $E_g^d - \Delta E_c - 0.3$  term is an estimation of the maximum open circuit voltage ( $V_{oc}$ ).<sup>8,10</sup> The integral in the numerator is the short circuit currency (EQE) of 100%,<sup>11</sup> and the integral in the denominator is the incident solar radiation ( $P_{solar}=1000 \text{ Wm}^{-2}$ ).<sup>12</sup>

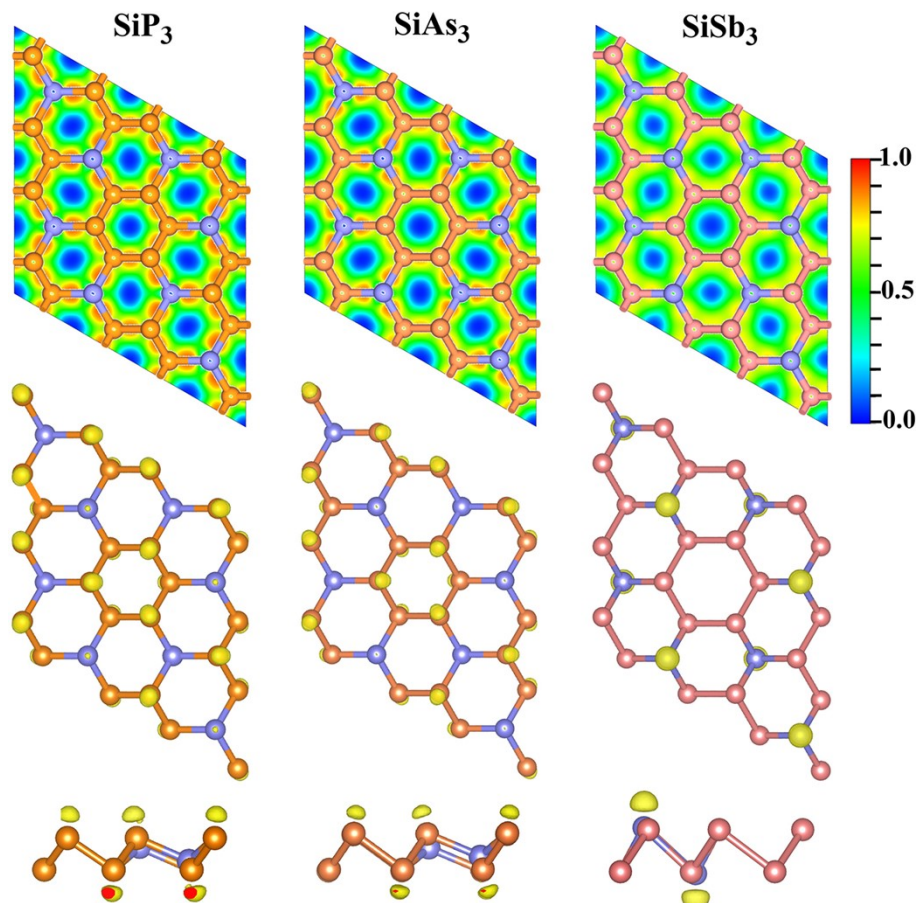


**Fig. S1** The 2D and 3D ELFs of monolayer  $\text{SiX}_3$  ( $\text{X}=\text{P}, \text{As}, \text{Sb}$ ) are presented.

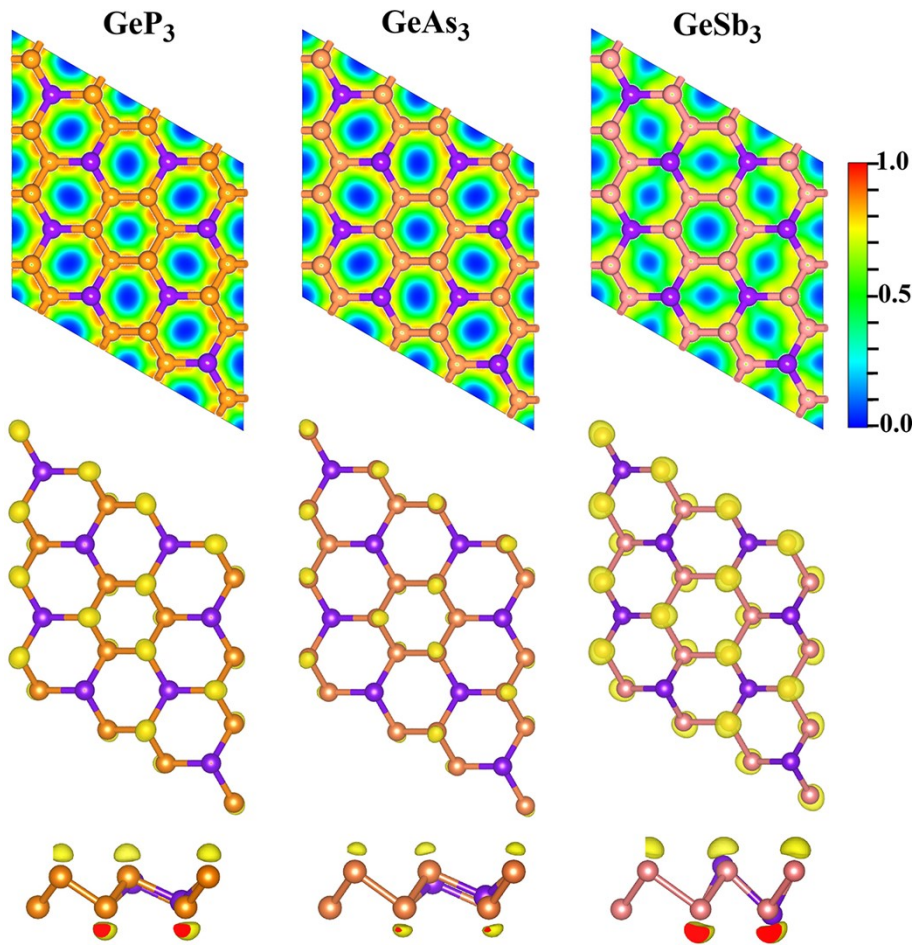


**Fig. S2** The 2D and 3D ELFs of monolayer  $\text{GeX}_3$  ( $\text{X}=\text{P}, \text{As}, \text{Sb}$ ) are presented.

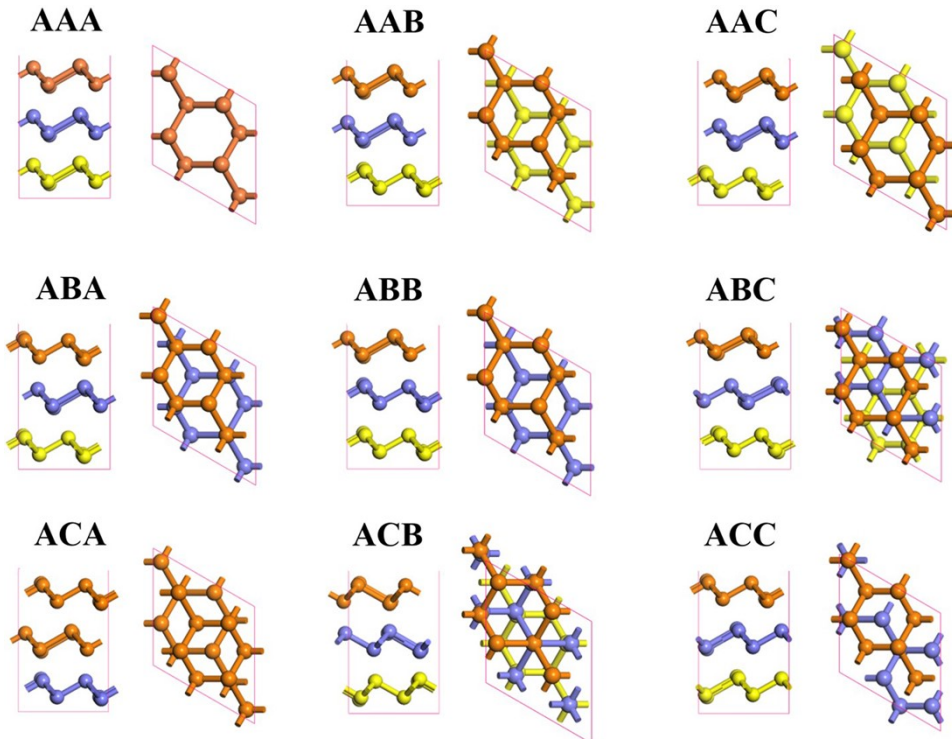


**Fig. S3** Side and top views of nine stacked (AAA, AAB, AAC, ABA, ABB, ABC, ACA and ACB) bulk  $\text{AX}_3$  ( $\text{X}=\text{P}, \text{As}, \text{Sb}$ ). The pink lines in the bottom panels of every stacked structure stand for the rhombus primitive cell.

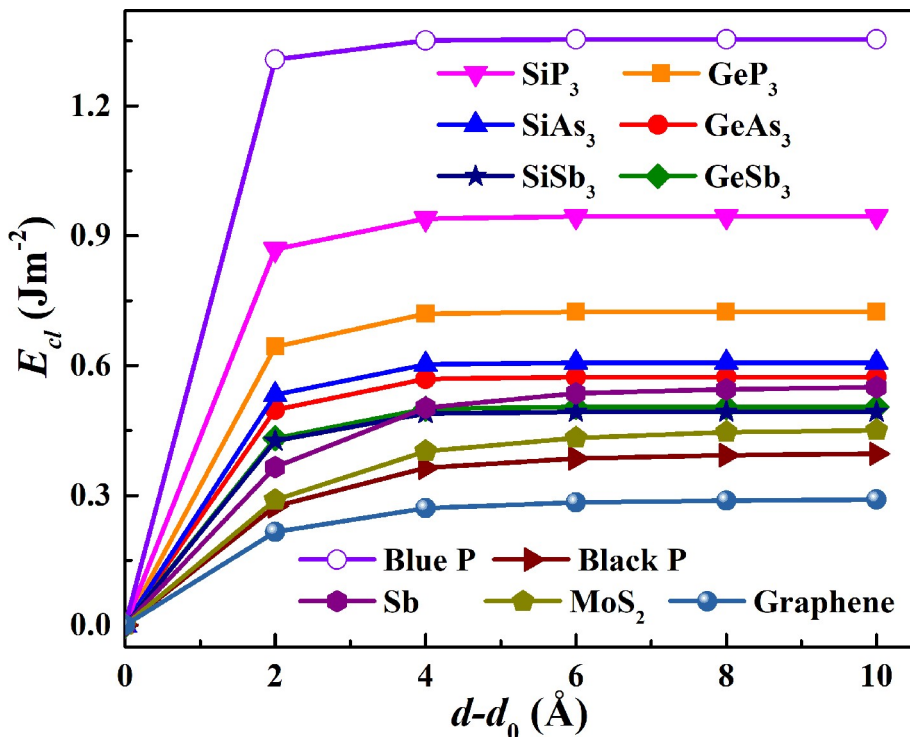


**Fig. S4** The cleavage energies of monolayer  $\text{AX}_3$ , coupled with blue phosphorene, black phosphorene, grey antimonene, monolayer MoS<sub>2</sub> and graphene for comparison.

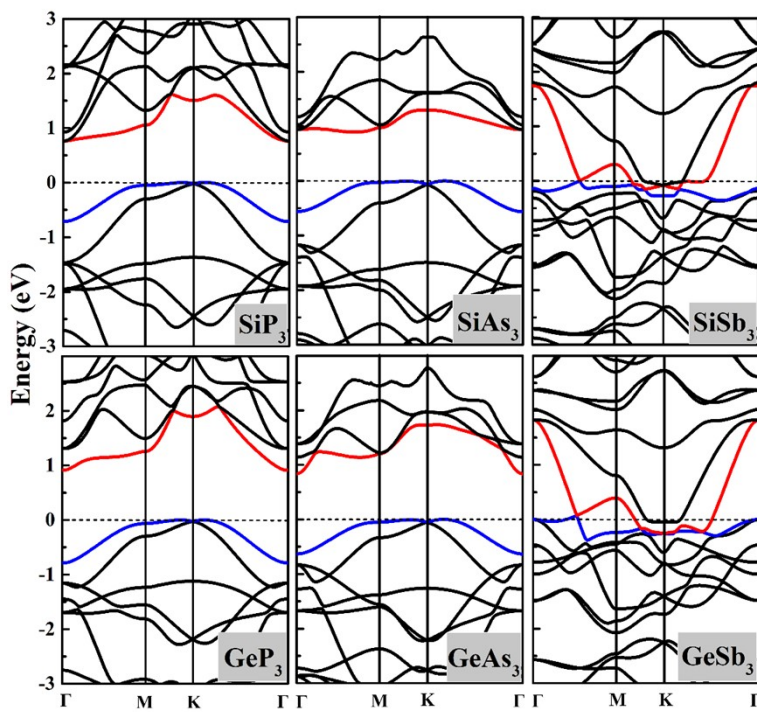


**Fig. S5** Electronic band structures of monolayer  $\text{AX}_3$  ( $\text{A}=\text{Si, Ge}$ ;  $\text{X}=\text{P, As, Sb}$ ). Red and blue lines represent the CB and VB near to the Fermi Level based on PBE functional, respectively.

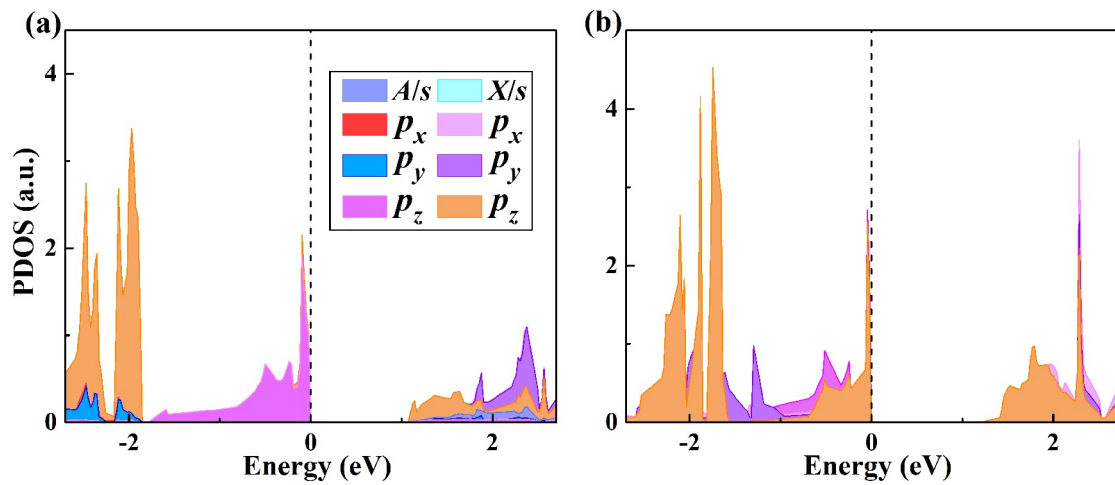


**Fig. S6** The projected density of states of monolayer  $\text{SiX}_3$  (a) and  $\text{GeX}_3$  (b) ( $\text{X}=\text{P, As}$ ).

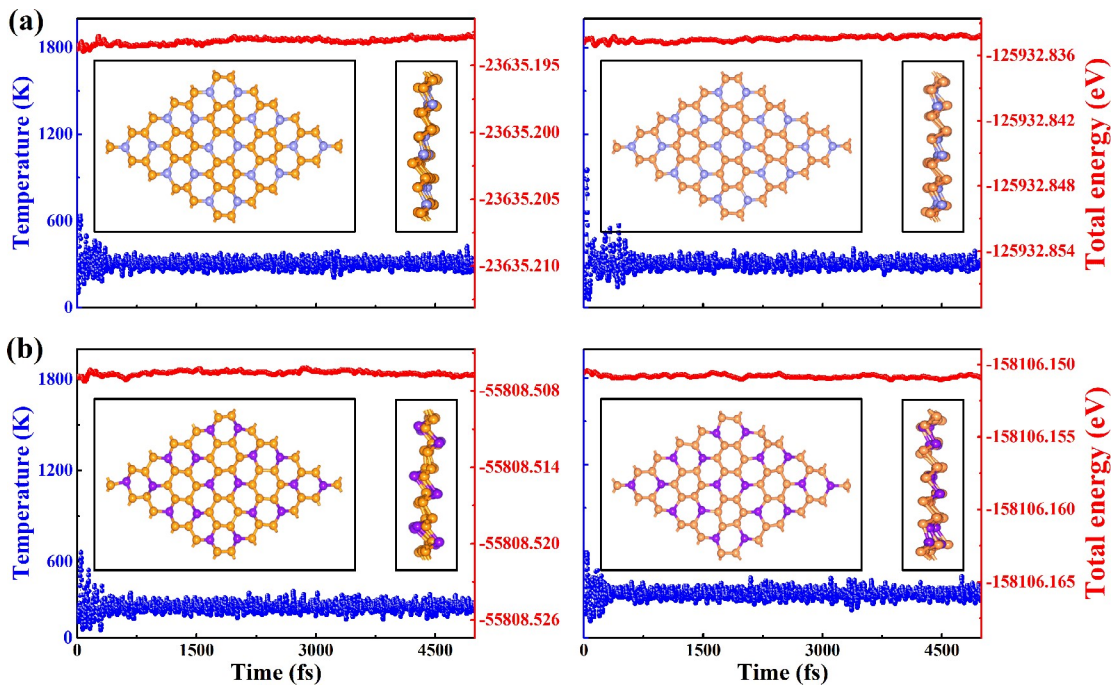


**Fig. S7** Temperature and total energy during an ab initio molecular dynamics (AIMD) simulation of monolayer  $\text{SiX}_3$  (a) and  $\text{GeX}_3$  (b) ( $\text{X}=\text{P}, \text{As}$ ) at 300 K. Inset: atomic structure after 5.0 ps.

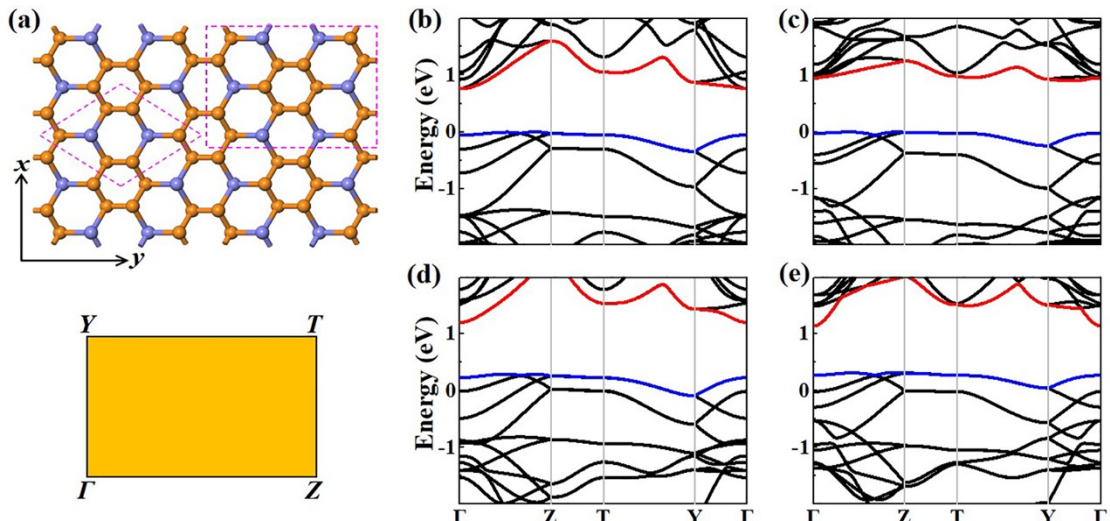


**Fig. S8** (a) Atomic structure model of monolayer  $\text{AX}_3$  ( $\text{X}=\text{P}, \text{As}$ ). The dashed lines represent the rhombus primitive cell and the rectangular supercell. Electronic band structures of monolayer  $\text{SiP}_3$  (b), and  $\text{SiAs}_3$  (c),  $\text{GeP}_3$  (d) and  $\text{GeAs}_3$  (e) in the orthogonal supercell.

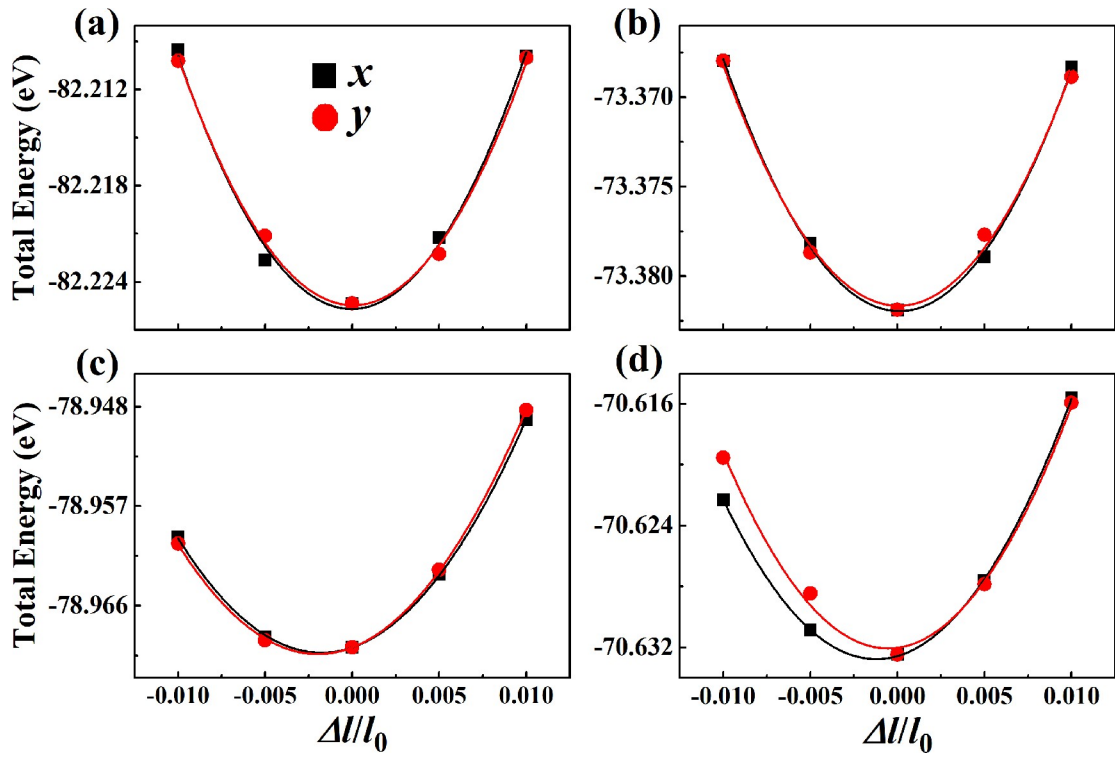


**Fig. S9** 2D elastic constant evaluation for the SiP<sub>3</sub> (a), SiAs<sub>3</sub> (b), GeP<sub>3</sub> (c) and GeAs<sub>3</sub> (d) monolayers. Total energy with respect to the lattice dilation  $\Delta l/l_0$ . The polynomial fit of the data gives the 2D elastic constant.

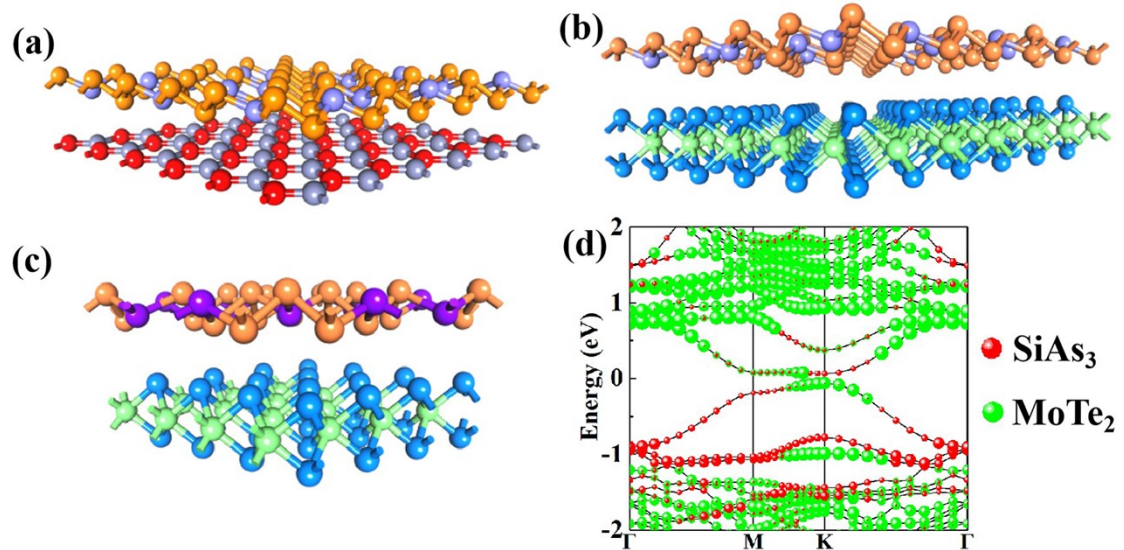


**Fig. S10** SiP<sub>3</sub>/ZnO (a), SiAs<sub>3</sub>/MoTe<sub>2</sub> (b) and GeAs<sub>3</sub>/WS<sub>2</sub> (c) type-II semiconductor heterojunctions. (d) Projected electronic structure of SiAs<sub>3</sub>/MoTe<sub>2</sub> heterojunction calculated using HSE06 functional.

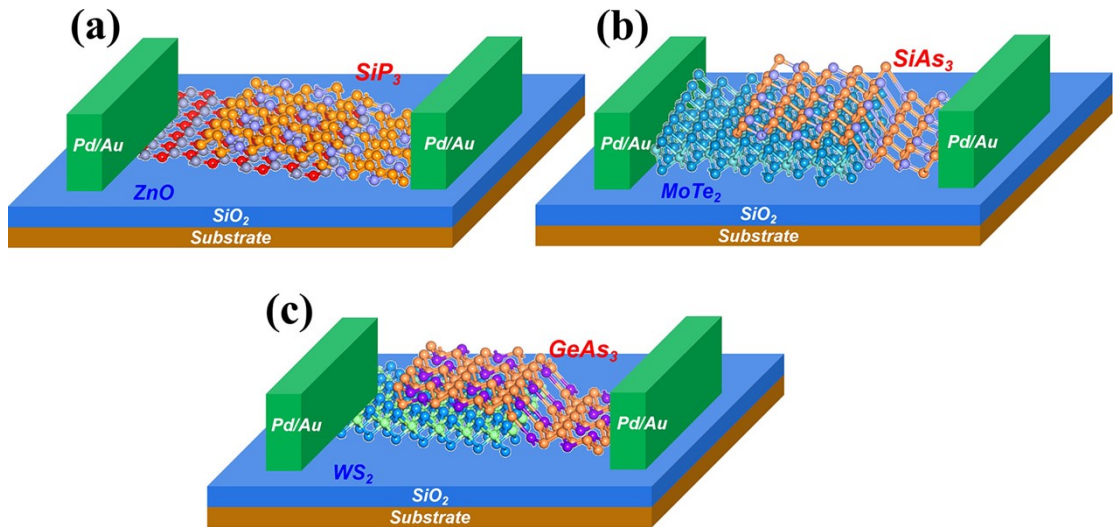


**Fig. S11** The devices structures of  $\text{SiP}_3$ - (a),  $\text{SiAs}_3$ - (b) and  $\text{GeAs}_3$ -based (c) single-junction SCs.

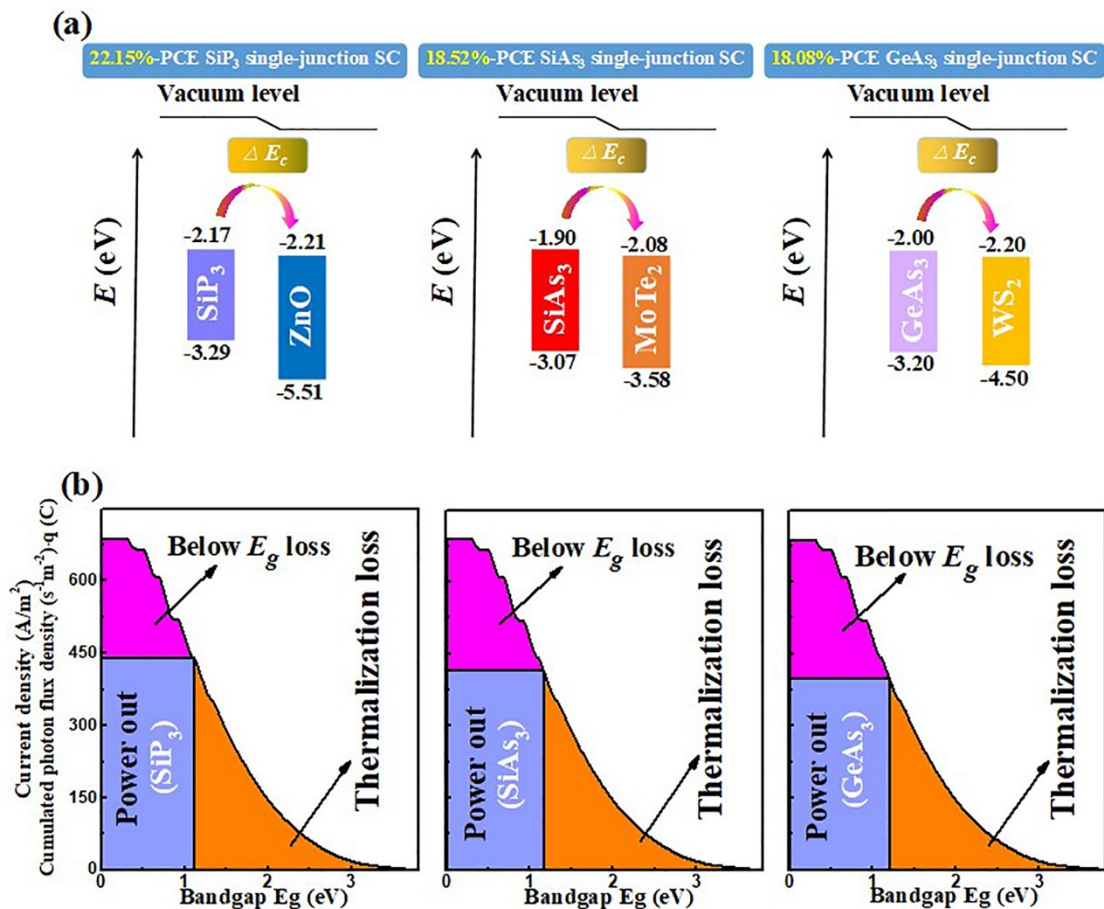


**Fig. S12** (a) Energy diagram of the band alignment (HSE06 functional) for  $\text{SiP}_3$ -,  $\text{SiAs}_3$ - and  $\text{GeAs}_3$ -based single-junction SCs with 22.15%, 18.52% and 18.08% efficiency, respectively. (b) Thermalization loss and below- $E_g$  loss in the  $\text{SiP}_3$ -,  $\text{SiAs}_3$ - and  $\text{GeAs}_3$ -based single-junction SCs.

**Table S1** Structural parameters and electronic properties for relaxed  $\text{AX}_3$  monolayers.

<b><math>\text{AX}_3</math> (A=Si, Ge; X=P, As, Sb) monolayers</b>											
	<i>a</i>	<i>h</i>	$l_{A-X}$	$l_{X-X}$	$E_{coh}$	$E^i_{PBE}$	$E^i_{HSE}$	$E^d_{HSE}$	$E_I$	$E_b$	<i>Q</i>
<b><math>\text{SiP}_3</math></b>	6.84	1.27	2.28	2.25	4.96	0.76	1.11	1.42	1.50	0.28	2.18
<b><math>\text{SiAs}_3</math></b>	7.33	1.49	2.40	2.51	4.41	0.89	1.17	1.22	1.64	0.59	1.14
<b><math>\text{SiSb}_3</math></b>	7.47	1.93	2.71	2.92	3.86	0	0	0	-	-	2.25
<b><math>\text{GeP}_3</math></b>	6.99	1.25	2.40	2.24	4.76	0.92	1.27	1.67	1.60	0.65	0.97
<b><math>\text{GeAs}_3</math></b>	7.46	1.47	2.51	2.50	4.19	0.84	1.20	1.50	2.02	0.42	0.55
<b><math>\text{GeSb}_3</math></b>	7.55	2.16	2.78	2.92	3.76	0	0	0	-	-	0.03

Lattice parameters  $a$ , bond lengths  $l_{A-X}$ ,  $l_{X-X}$  in units of Å. Calculated indirect PBE bandgap  $E^i_{PBE}$  and HSE06 bandgap  $E^i_{HSE}$  associate with direct HSE06 bandgap  $E^d_{HSE}$  (in units of eV). The first bright excitonic energies (optical gap,  $E_I$  in units of eV) based on GW+BSE calculation. The cohesive energies  $E_{coh}$  (in units of eV/atom) are computed in reference to the spin-polarized A and X atoms. The exciton binding energies  $E_b$  in units of eV. Bader charges  $Q$  in units of e transformed from A to X atoms, while Sb to Si atom in monolayer  $\text{SiSb}_3$ .

**Table S2.** Calculated cohesive energy differences ( $\Delta E_{coh}$ ) are given in units of eV.  $\Delta E_{coh}$  is based on the ABC stacking  $\text{AX}_3$  monolayer calculated with PBE functional.

	<b><i>AAA</i></b>	<b><i>AAB</i></b>	<b><i>AAC</i></b>	<b><i>ABA</i></b>	<b><i>ABB</i></b>	<b><i>ABC</i></b>	<b><i>ACA</i></b>	<b><i>ACB</i></b>	<b><i>ACC</i></b>
<b><math>\text{SiP}_3</math></b>	0.007	0.097	0.097	0.097	0.097	0	0.097	0.114	0.097
<b><math>\text{SiAs}_3</math></b>	0.059	0.051	0.051	0.051	0.051	0	0.051	0.047	0.051
<b><math>\text{SiSb}_3</math></b>	0.056	0.060	0.060	0.060	0.060	0	0.060	0.067	0.060
<b><math>\text{GeP}_3</math></b>	0.029	0.088	0.088	0.088	0.088	0	0.088	0.118	0.088
<b><math>\text{GeAs}_3</math></b>	0.127	0.065	0.065	0.065	0.235	0	0.065	0.087	0.065
<b><math>\text{GeSb}_3</math></b>	0.071	0.065	0.065	0.065	0.065	0	0.065	0.104	0.065

**Table S3** Effective mass  $m_i^*/m_0$ , DP constant  $E_{Ii}$  in eV, elastic constant  $C_{2D}$  in Jm<sup>-2</sup>, and carrier mobility  $\mu$  in cm<sup>2</sup>V<sup>-1</sup>s<sup>-1</sup>, at 300 K for electrons and holes in monolayer  $\text{AX}_3$  (A=Si, Ge; X=P, As). (x=zigzag, y=armchair)

<b>Models</b>		$m_x^*/m_0$	$m_y^*/m_0$	$E_{Ix}$	$E_{Iy}$	$C_{x/2D}$	$C_{y/2D}$	$\mu_{x/2D}$	$\mu_{y/2D}$
<b><math>\text{SiP}_3</math></b>	<b><i>e</i></b>	0.46	0.18	12.24	8.66	61.86	60.25	66.71	334.05
	<b><i>h</i></b>	0.40	0.54	1.98	2.18	61.86	60.25	1798.31	1079.79
<b><math>\text{SiAs}_3</math></b>	<b><i>e</i></b>	1.40	0.03	8.05	2.09	47.18	46.28	51.30	31447.40
	<b><i>h</i></b>	0.62	0.93	1.49	0.84	47.18	46.28	955.00	1967.00
<b><math>\text{GeP}_3</math></b>	<b><i>e</i></b>	0.26	0.26	5.99	5.70	57.72	58.30	519.11	578.83

<i>GeAs<sub>3</sub></i>	<i>h</i>	0.56	1.03	2.45	2.23	57.72	58.30	488.15	322.01
<i>Si<sup>13</sup></i>	<i>e</i>	0.08	0.08	13.22	13.12	44.91	48.99	813.40	900.70
<i>Si<sup>13</sup></i>	<i>h</i>	0.68	0.91	0.56	0.54	44.91	48.99	5768.00	5036.00
	<i>e</i>								1,450
	<i>h</i>								450

**Table S4** Confirmed existing SCs and the PCE measured under the global AM1.5 spectrum (1000 Wm<sup>-2</sup>).

No.	Cell Structure	PCE (%)	References	Year
1	<b>SiP<sub>3</sub>/ZnO, SiAs<sub>3</sub>/MoTe<sub>2</sub> and GeAs<sub>3</sub>/WS<sub>2</sub>-based PV cells</b>	<b>22.15/18.52/18.08</b>	<b>This work</b>	
2	BTPV-4F/PTB7-Th tandem SC	16.4	14	2021
3	n-CdS/p-Si heterojunction SC	18.72	15	2021
4	$\alpha$ -AsP/GaN SC	22.1	16	2016
5	CH <sub>3</sub> NH <sub>3</sub> PbI <sub>3</sub> SC	21	17	2014
6	MoSe <sub>2</sub> / $\Psi$ -phosphorene SC	20.26	18	2017
7	TiNF/TiNCl SC	22	19	2018
8	Ti <sub>3</sub> C <sub>2</sub> T <sub>x</sub> -based silicon heterojunction SCs	20	20	2022
9	functionalized silicene/graphene SC	23.34	21	2021
10	Te/WTe <sub>2</sub> , Te/MoTe <sub>2</sub> heterojunction SCs	22.5/20.1	22	2019
11	$\alpha$ -Sb <sub>2</sub> TeSe <sub>2</sub> /HfSe <sub>2</sub> , $\beta$ -Sb <sub>2</sub> TeSe <sub>2</sub> /BiOI SCs	22.5/20.3	23	2021

## References

1. M. Gajdoš, K. Hummer, G. Kresse, J. Furthmüller, F. Bechstedt, *Phys. Rev. B*, 2006, **73**, 045112.
2. H. Shi, M. Chu, P. Zhang, *J. Nucl. Mater.*, 2010, **400**, 151-156.
3. S. Albrecht, L. Reining, R. Del Sole and G. Onida, *Phys. Rev. Lett.*, 1998, **80**, 4510-4513.
4. M. S. Hybertsen and S. G. Louie, *Phys. Rev. B*, 1986, **34**, 5390-5413
5. M. Rohlfing and S. G. Louie, *Phys. Rev. Lett.*, 1998, **81**, 2312-2315.
6. S. Ismail-Beigi, *Phys. Rev. B*, 2006, **73**, 233103.
7. J. Bardeen and W. Shockley, *Phys. Rev.*, 1950, **80**, 72.
8. M. C. Scharber, D. Mühlbacher, M. Koppe, P. Denk, C. Waldauf, A. J. Heeger and C. J. Brabec, *Adv. Mater.*, 2006, **18**, 789-794.
9. The AM1.5G spectrum was taken from the NREL website: <http://rredc.nrel.gov/solar/spectra/am1.5> and integrated with the trapezoid rule.
10. M. D. Perez, C. Borek, S. R. Forrest and M. E. Thompson, *J. Am. Chem. Soc.*, 2009, **131**, 9281-9286.
11. M. Bernardi, M. Palummo and J. C. Grossman, *ACS Nano*, 2012, **6**, 10082-10089.
12. J. D. Servaites, M. A. Ratner and T. J. Marks, *Appl. Phys. Lett.*, 2009, **95**, 163302.
13. C. Jacoboni, C. Canali, G. Ottaviani and A. A. Quaranta, *Solid State Electron.*, 1977, **20**, 77-89.
14. Z. Jia, S. Qin, L. Meng, Q. Ma, I. Angunawela, J. Zhang, X. Li, Y. He, W. Lai, N. Li, H. Ade, C. J. Brabec and Y. Li, *Nat. Commun.*, 2021, **12**, 178.
15. S. Srivastava, S. Singh and V. K. Singh, *Opt. Matter.*, 2021, **111**, 110687.
16. M. Xie, S. Zhang, B. Cai, Y. Huang, Y. Zou, B. Guo, Y. Gu and H. Zeng, *Nano Energy*, 2016, **28**, 433-439.
17. W.-J. Yin, T. Shi and Y. Yan, *Adv. Mater.*, 2014, **26**, 4653-4658.
18. H. Wang, X. Li, Z. Liu and J. Yang, *Phys. Chem. Chem. Phys.*, 2017, **19**, 2402-2408.
19. Y. Liang, Y. Dai, Y. Ma, L. Ju, W. Wei and B. Huang, *J. Mater. Chem. A*, 2018, **6**, 2073-2080.
20. E. Aydin, J. K. El-Demellawi, E. Yarali, F. Aljamaan, S. Sansoni, A. U. Rehman, G. Harrison, J. Kang, A. El Labban, M. De Bastiani, A. Razzaq, E. Van Kerschaver, T. G. Allen, O. F. Mohammed, T. Anthopoulos, H. N. Alshareef and S. De Wolf, *ACS Nano*, 2022, **16**, 2419-2428.
21. H. Abdelsalam, M. M. Atta, W. Osman and Q. Zhang, *J. Colloid Interf. Sci.*, 2021, **603**, 48-57.
22. K. Wu, H. Ma, Y. Gao, W. Hu and J. Yang, *J. Mater. Chem. A*, 2019, **7**, 7430-7436.
23. C. Wang, Y. Jing, X. Zhou and Y. F. Li, *ACS Omega*, 2021, **6**, 20590-20597.